ADVANCED FUNCTIONAL MATERIALS
www.afm-journal.de

High-Throughput Screening of Self-Healable Polysulfobetaine Hydrogels and their Applications in Flexible Electronics

Yan Ding, Haoqi Tang, Chaohong Zhang, Weixuan Li, Gang Li, Yuan Zhang, Chen Xu, Fu Zhao, Qiongyu Guo, Chuan Fei Guo,* and X.-D. Xiang**

Hydrogels are promising materials in the applications of wound adhesives, wearable electronics, tissue engineering, implantable electronics, etc. The properties of a hydrogel rely strongly on its composition. However, the optimization of hydrogel properties has been a big challenge as increasing numbers of components are added to enhance and synergize its mechanical, biomedical, electrical, and self-healable properties. Here in this work, it is shown that high-throughput screening can efficiently and systematically explore the effects of multiple components (at least eight) on the properties of polysulfobetaine hydrogels, as well as provide a useful database for diverse applications. The optimized polysulfobetaine hydrogels that exhibit outstanding self-healing and mechanical properties, have been obtained by high-throughput screening. By compositing with poly(3,4-ethylenedioxythiophene):polystyrene sulfonate (PEDOT:PSS), intrinsically self-healable and stretchable conductors are achieved. It is further demonstrated that a polysulfobetaine hydrogel-based electronic skin, which exhibits exceptionally fast self-healing capability of the whole device at ambient conditions. This work successfully extends high-throughput synthetic methodology to the field of hydrogel electronics, as well as demonstrates new directions of healable flexible electronic devices in terms of material development and device design.

1. Introduction

Increasing numbers of components are added to hydrogels to broaden their unique functions, as hydrogels are applied to more and more fields.[1–6] An efficient screening method is thus urgently required to accelerate the composition optimization of hydrogels. The materials genome has achieved great success in life science credited to its capability to rapidly and accurately generate numerous results, which are otherwise arduous using traditional methods.[7,8] Nevertheless, materials science has not yet been benefited from high-throughput technologies (HTTs) as much as life science has.[9] High-throughput screening technology in materials science was initiated by Xiang and Schultz in 1995, which involved parallel preparation of superconducting materials through the combination of thin film deposition and physical masking techniques.[10] This technology was soon improved and applied to the discovery of other new

Y. Ding, Dr. H. Tang, Dr. C. Zhang, Dr. W. Li, G. Li, Y. Zhang, Dr. C. Xu, Dr. F. Zhao, Prof. C. F. Guo, Prof. X.-D. Xiang
Department of Materials Science and Engineering
Southern University of Science and Technology
Shenzhen, Guangdong 518055, China
E-mail: chaohong_zhang@pku.edu.cn; guocf@sustech.edu.cn; xiangxd@sustech.edu.cn

Dr. C. Zhang
School of Advanced Materials
Peking University Shenzhen Graduate School
Shenzhen, Guangdong 518055, China

Dr. C. Xu, Dr. F. Zhao
SUSTech Academy for Advanced Interdisciplinary Studies
Southern University of Science and Technology
Shenzhen, Guangdong 518055, China

The ORCID identification number(s) for the author(s) of this article can be found under https://doi.org/10.1002/adfm.202100489.

DOI: 10.1002/adfm.202100489

Prof. Q. Guo
Department of Biomedical Engineering
Southern University of Science and Technology
Shenzhen, Guangdong 518055, China

Prof. X.-D. Xiang
Department of Physics
Southern University of Science and Technology
Shenzhen, Guangdong 518055, China

Prof. X.-D. Xiang
Guangdong Provincial Key Laboratory of Energy Materials for Electric Power
Academy for Advanced Interdisciplinary Studies
Southern University of Science and Technology
Shenzhen, Guangdong 518055, China

Prof. X.-D. Xiang
Guangdong-Hong Kong-Macao Joint Laboratory for Photonic-Thermal-Electrical Energy Materials and Devices
Academy for Advanced Interdisciplinary Studies
Southern University of Science and Technology
Shenzhen, Guangdong 518055, China

materials such as magnetoresistance materials,[11] phosphors,[12] and solution-phase synthesis of luminescent materials.[13] To date, high-throughput technologies have been developed and applied to a wide variety of materials including catalysts,[14] electronics, functional materials,[15,16] and others.[17,18] In the field of polymer materials which was initially considered highly challenging for HTTs, researchers have managed to employ HTTs to discover novel polymerization catalysts,[19] polymers,[20] and polymer blends.[21]

Hydrogels are a group of crosslinking polymers with exciting applications in emerging fields such as soft electronics and tissue engineering.[1,2] Nevertheless, a high-throughput screening method has not yet been utilized for the discovery of high-performance hydrogels. In fact, high-throughput experimentation is highly suitable for hydrogel synthesis because stirring and post-treatment are usually not mandatory in the process. High-throughput screening methods can greatly benefit the field of hydrogel development and application from at least three aspects. First, increasing numbers of components are added to enhance and synergize the mechanical, biomedical, electrical, and self-healable properties of hydrogels. Such material discovery and optimization are a labor-intensive work if everything is done manually. By introducing the high-throughput experimentation, however, significant labor and costs are saved and the timescale is greatly shortened. Second, as sample preparation and characterization are conducted systematically at a time via HTTs, the environmental consistency of sample preparation and characterization is guaranteed, thereby greatly reducing the interference of external environmental factors. Third, the databases generated by HTTs are trustworthy and useful for future reference and machine learning due to the above mentioned advantages.

Hydrogels usually experience significant deformations and even failure over their service life. Therefore, it is necessary to render hydrogels appropriate mechanical properties and, especially, spontaneous self-healing capability.[22] Self-healing can be realized through reversible bonding, such as imine bond,[23] acythydrazone bond,[24] ionic bonding,[25] hydrophobic association (HA),[26] host–guest interaction,[27] and metallic coordination.[28] Among the non-covalent reversible bonds, ionic bonding is faster in self-healing and stronger in strength than others.[29] Polybetaines materials that have cationic and anionic groups in the same monomer unit have attracted broad attentions in recent years.[30,31] Different from other physically crosslinked hydrogels that heal only at freshly-cut surfaces, polybetaines hydrogels can self-heal time-independently under the protection of a hydrated layer at fractured surfaces due to their super-hydrophilicity.[30–32]

However, achieving polybetaines hydrogels with desired self-healing efficiency as well as satisfying mechanical properties remains a challenge. On one hand, chemical crosslinking improves mechanical properties, however, the increased crosslinker ratio results in diminished flexibility and lower self-healing efficiency owing to the lower mobility of zwitterionic pendant chains.[32,33] On the other hand, hydrophobic association is an ideal candidate serving as protective bonding to facilitate energy dissipation for ionic-bond-based hydrogels, simultaneously enhancing mechanical and self-healing properties.[34,35] Additionally, it was reported that anionic, cationic, and amphoteric surfactants interact differently with ionic polymers, resulting in dissimilar polymer networks and hydrogel properties.[36,37] Assisting with surfactants, Okay's group incorporated hydrophobic sequences into poly(*N*,*N*-dimethylacrylamide) and poly(acrylic acid) chains, and found that elastic moduli and self-healing performance were enhanced concurrently with increasing hydrophobic crosslinking density.[38,39] However, to further create larger surfactant micelles to introduce more hydrophobic monomers, it usually requires small molecular electrolyte (such as sodium chloride) which deteriorates the self-healing property due to ionic shielding.[40,41]

Here in this work, we synthesized polysulfobetaine hydrogels mediated by hydrophobic association with 3-dimethyl-2-(2-methylprop-2-enoyloxy)ethyl azaniumyl propane-1-sulfonate (DMAPS) as the zwitterionic monomer, poly(ethylene glycol) diacrylate (PEGDA) as the crosslinker, 2,2,2-trifluoroethyl methacrylate (FMA) as the hydrophobic monomer, and cetyltrimethylammonium chloride (CTAC), sodium dodecyl sulfate (SDS), or lauryl betaine (BS-12) as the cosolvent. DMAPS monomer provides ionic bonds to obtain hydrogels with excellent mechanical and self-healing properties. PEGDA with different molecular weight were selected to investigate the effects of chain length of chemical crosslinkers on mechanical properties, which has not been reported elsewhere. We further introduced FMA, a small hydrophobic monomer which does not require the assisting dissolubility from inorganic salts such as NaCl dramatically deteriorating the self-healing properties resulting from ionic shielding.

In total, by using the HTT, more than 150 hydrogels in two batches were successfully attained and the effects of the eight components on hydrogel properties were investigated systematically. The optimized polysulfobetaine hydrogels exhibited an elongation at fracture of ≈4000%, a strength at break of ≈400 kPa, and a self-healing efficiency of ≈100%. Furthermore, by compositing poly(3,4-ethylenedioxythiophene):polystyrene sulfonate (PEDOT:PSS), the self-healable and stretchable polysulfobetaine hydrogels were further functionalized with improved electrical conductance which could be restored immediately as fractured segments are reconnected. In addition, polysulfobetaine hydrogel-based capacitive-type sensors were fabricated, and the sensors could recover rapidly from complete cutting off throughout the whole devices. The high-throughput screening method is also expected to be extended to other hydrogel systems for high-performance hydrogel electronics and beyond.

2. Results and Discussion

A homemade syringe-based multi-channel feeding device was utilized to perform high-throughput synthesis of the polymer hydrogels (**Figure 1**a). Chemical structures of the main components in the study are shown in Figure 1b. The system consists of eight components: a zwitterionic monomer DMAPS, three crosslinkers PEGDA, a hydrophobic monomer FMA, and surfactants CTAC, SDS, and BS-12. The high-throughput synthesis of the polysulfobetaine hydrogels includes three simple steps. First, reagents were dissolved in water separately as stock solutions. Second, the stock solutions and deionized water were filled

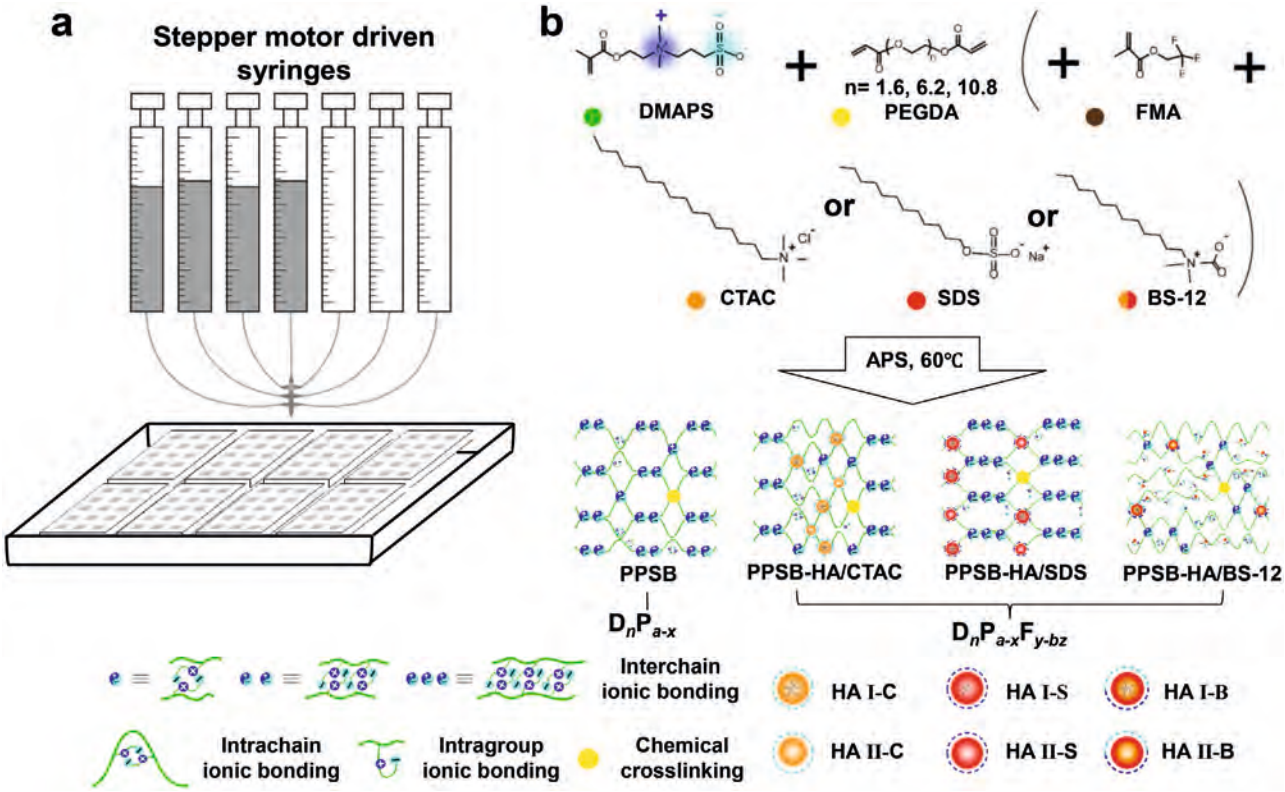

Figure 1. a) Illumination of high-throughput multi-channel feeding device. b Reaction scheme for the synthesis: chemical structures of zwitterionic monomer DMAPS, crosslinker PEGDA, hydrophobic monomer FMA and surfactants (CTAC, SDS, and BS-12); network structures of PPSB and PPSB-HA hydrogels (HA I micelles contain poly(FMA) and surfactants while HA II micelles contain pure surfactant molecules).

into separated syringes but delivered simultaneously and quantitatively into discrete reaction vessels under an injection program, to realize the high-efficient feeding of over 100 formulas. Next, the reaction vessels were placed in a 60 °C water bath under nitrogen atmosphere for 18 h for different formulas to form hydrogels. The multi-channel feeding mode accelerates the delivery of diversified components required for synergizing the multiplex properties of hydrogels. Two types of zwitterionic hydrogels were attained: PEGDA crosslinked polysulfobetaine hydrogels (PPSB) that contain pure ionic bonds as dynamic interactions; PPSB-HA series of hydrogels that contain both ionic bonds and hydrophobic association as dynamic interactions, including PPSB-HA/CTAC, PPSB-HA/SDS, and PPSB-HA/BS-12.

We first conducted the high throughput preparation of the PPSB hydrogels. Key parameters include the concentration of DMAPS (n), molecular weight of PEGDA (a), and crosslinking concentration (x) of the PPSB hydrogels (D_nP_{a-x}). As presented in **Table 1**, the DMAPS concentration gradient of 0.5 M is chosen because if the gradient of DMAPS concentration is small (e.g., 0.2 M), the differences in mechanical properties of the hydrogels are negligible according to our pre-experiments; PEGDAs with a molecular weight of 200, 400, and 600 were employed to investigate the influence of chain length and concentration of crosslinkers on mechanical properties; chemical crosslinking concentration varied with different combinations of DMAPS concentration and PEGDAs. The interest lies not only in finding the lowest chemical crosslinking concentration but also in exploring mechanical properties from a wide range of material concentrations to deliver a valuable database. Altogether 107 PPSB material combinations were examined, among

Table 1. Combinatorial libraries of monomer and crosslinkers for high-throughput synthesis.

Molar percentage [mol%][a]		DMAPS concentration [mol L^{-1}]		
		0.5	1.0	1.5
PEGDA	P200	0.5,[b] 1.0, 1.5, 2.0, 2.5, 3.0, 3.5, 4.0, 5.0, 6.0, 8.0	0.3, 0.5, 1.0, 1.5, 2.0, 2.5, 3.0, 3.5, 4.0, 5.0, 6.0	0.1, 0.2, 0.4, 0.6, 0.8, 1.2, 1.6, 2.0, 2.5, 3.0, 4.0
	P400	0.3, 0.5, 1.0, 1.5, 2.0, 2.5, 3.0, 3.5, 4.0, 5.0, 6.0	0.2, 0.4, 0.8, 1.2, 1.6, 2.0, 2.5, 3.0, 3.5, 4.5	0.1, 0.2, 0.4, 0.6, 0.8, 1.0, 1.2, 1.6, 2.0, 2.5, 3.0
	P600	0.2, 0.4, 0.6, 0.8,1.2, 1.6, 2.0, 2.5, 3.0, 4.0, 5.0, 6.0, 7.0	0.1, 0.2, 0.3, 0.4, 0.6, 0.8, 1.0, 1.2, 1.6, 2.0, 2.5, 3.0, 3.5, 4.5, 6.0	0.05, 0.1, 0.2, 0.3, 0.4, 0.5, 0.6, 0.8, 1.0, 1.5, 2.0, 2.5, 3.0, 4.0

[a]11 + 11 + 11 + 11 + 10 + 11 + 13 + 15 + 14 = 107 combinations and stoichiometries; [b]gelation did not occur for combinations with molar percentage of PEGDA underline.

which 96 samples were successfully gelated. Generally, material systems with higher DMAPS concentrations or longer PEGDA chains require lower crosslinker contents for gelation. After gelation, the as-prepared samples were kept at 25 °C and 80% relative humidity (RH) for 48 h before subjected to uniaxial tensile test.

The components of the PPSB hydrogels significantly affect their mechanical properties as expected, as summarized in **Figure 2** and Figures S1–S4, Supporting Information. Here the effects of the concentration of DMAPS and PEGDAs are well studied. Figure 2a and Figure S3, Supporting Information depict that higher DMAPS concentration leads to reduced elongation at break (ε_b). The data show that ε_b decreases from 1300% for $D_{0.5}P_{600-0.4}$ to 620% for $D_{1.5}P_{600-0.4}$. On the contrary, Young's modulus (E) of the materials increases with increasing DMAPS concentration. In addition, strength at break (σ_b) fluctuates from 200 to 450 kPa with varying P600 and DMAPS combinations. Increasing the monomer concentration leads to enhanced ionic contact with neighboring monomer units and other polymer chains, thereby enhancing physical crosslinking and restricting polymer network deformation. Figure 2b reveals that longer PEGDA chain length results in smaller ε_b. For example, ε_b is around 2000% for $D_{1.5}P_{200-0.2}$, whereas ε_b decreases to ≈1200% for $D_{1.5}P_{400-0.2}$ and further lowers to ≈800% for $D_{1.5}P_{600-0.2}$. Generally, E exhibits the opposite trend compared with ε_b concerning the effects of PEGDA chain length. The phenomenon can be explained by the entanglement of PEGDA and poly(DMAPS) chains as illustrated in Figure S5, Supporting Information. These entanglements act as effective crosslinking points for the polymer network, hardening the hydrogels. Crosslinkers with longer chains cause more severe chain entanglement, therefore longer PEGDA leads to stronger resistance against deformation and lower stretchability. Both Figure 2a,b demonstrate that ε_b decreases with increasing PEGDA crosslinker content while E exhibits an opposite tendency. For example, ε_b of $D_{0.5}P_{600-0.4}$ hydrogel is ≈1300% with a P600 content of 0.4 mol%, and gradually decreases to ≈400% when P600 content raises up to 3.0 mol% (Figure 2a).

Fracture energy (U), or the quantity of toughness, represents the comprehensive mechanical properties of the hydrogels. Therefore, U is selected as a key criterion for the optimization of the PPSB hydrogels in this work. U fluctuates along with various combinations of monomer concentration and crosslinker content (Figure 2c). For D_1P_{600-x} hydrogels, U remains at a high level of ≈1100–1200 $kJ \cdot m^{-3}$ over a wide range of P600 content (≈0.2–1.0 mol%). Therefore, $D_{1.0}P_{600-0.3}$ was selected for further optimization by adding hydrophobic segments.

For the second batch of synthesis (PPSB-HA hydrogels), a short but highly hydrophobic monomer FMA was introduced by micellar polymerization without the assistance of salt which is harmful to self-healing properties. As surfactant molecules will diminish the self-healing performance, the concentration of 18 w/v% was the highest concentration of surfactants. When 6 or 18 w/v% surfactant was added, the highest concentration of FMA dissolved in the stock solution is 50 mol% related to DMAPS. Variables in this batch of hydrogels ($D_1P_{600-0.3}F_{y-bz}$) were FMA content (y: from 5 to 50 mol%), category of surfactants (b: C/S/B, CTAC with a cationic head, SDS with an anionic head, and BS-12 with a zwitterionic head), and surfactant content (z: 6, 12, or 18 w/v%) as listed in **Table 2**. Totally 58 combinations were explored and all formulas were gelated.

The mechanical properties of the as-made hydrogels are summarized in Figure 2c,d and Figure S6, Supporting Information. For the CTAC assisting system, the addition of FMA greatly increases ε_b compared with the control hydrogel ($D_1P_{600-0.3}$). With a small amount of FMA (5 mol% to DMAPS), ε_b of the hydrogel increases from 1300% (for $D_1P_{600-0.3}$) to ≈4000% (for $D_1P_{600-0.3}F_{5-Cz}$). Elongation at break gradually decreases with increasing amount of FMA but is still higher than that of $D_1P_{600-0.3}$ except for the $D_1P_{600-0.3}F_{50-Cz}$ samples which are inhomogeneous hydrogels because of the incomplete dissolution of FMA. The strength at break of PPSB-HA/CTAC hydrogels usually remains as high as that of $D_1P_{600-0.3}$. Different from PPSB-HA/CTAC hydrogels, elongation at break of PPSB-HA/SDS hydrogels stays similar to that of $D_1P_{600-0.3}$ hydrogel. However, the PPSB-HA/SDS hydrogels exhibit a higher σ_b of over 380 kPa on average, thus effectively toughening the hydrogels. Interestingly, the amount of FMA and SDS seems to play an insignificant role to the toughening of the hydrogels, indicating a toughening mechanism different from CTAC. The certainty of the phenomena was verified by another batch of PPSB-HA/SDS hydrogels based on $D_{1.5}P_{200-0.4}$ (depicted in Figure S7, Supporting Information). For PPSB-HA/BS-12 hydrogels, elongation at break is merely slightly improved compared with that of the $D_1P_{600-0.3}$ hydrogel. Nevertheless, the reduced σ_b results in a poor fracture energy.

The self-healing efficiency of hydrogels is quantitatively defined as the elongation ratio at break between the self-healed and original hydrogels. The hydrogels were cut into two pieces, reconnected immediately, kept in 25 °C and 80% RH for 24 h, and then subjected to uniaxial tensile. As shown in **Figure 3**a, the $D_1P_{600-0.3}$ hydrogel exhibits a favorable self-healing efficiency of 88%. Such high efficiency lies in the reversible electrostatic interaction of oppositely charged pendent ions along the polymer chains. The PPSB-HA/CTAC hydrogels with 6 w/v% CTAC display an average self-healing efficiency of 85%, which is as excellent as the $D_1P_{600-0.3}$ sample; however, self-healing performance is gradually undermined with increasing amount of CTAC, dropping to around ≈30–60% when adding 12 w/v% CTAC, and to ≈10–25% with 18 w/v% CTAC. The PPSB-HA/SDS hydrogels exhibit high self-healing efficiency (≈80–90%) with ≈6–12 w/v% SDS, but it drops to ≈40–60% when the SDS content increases to 18 w/v%. As shown in Figure S8, Supporting Information, the stress–strain curves of the original and self-healed hydrogels are well overlapped, indicating the full recovery of mechanical properties. By contrast, all PPSB-HA/BS-12 hydrogels suffer from unfavorable self-healing efficiency, which is typically lower than 20%. As described in Figure 3b, the well-healed hydrogels ($D_1P_{600-0.3}$, $D_1P_{600-0.3}F_{5-C6}$, and $D_1P_{600-0.3}F_{5-S6}$) are able to mold the cylindrical shape of the syringe, exhibiting self-remolding characteristics. The self-remolding property indicates that the PPSB, PPSB-HA/CTAC, and PPSB-HA/SDS hydrogels can self-heal on various surfaces and independent of the time the cut-surface exposed to air.[32] The self-healing efficiency can further increase by raising the RH of the atmosphere. The $D_1P_{600-0.3}$, $D_1P_{600-0.3}F_{5-C6}$, and $D_1P_{600-0.3}F_{5-S6}$ hydrogels all achieve complete recovery of tensile strain in 2 h when the RH increases to 90% (Figure 3c).

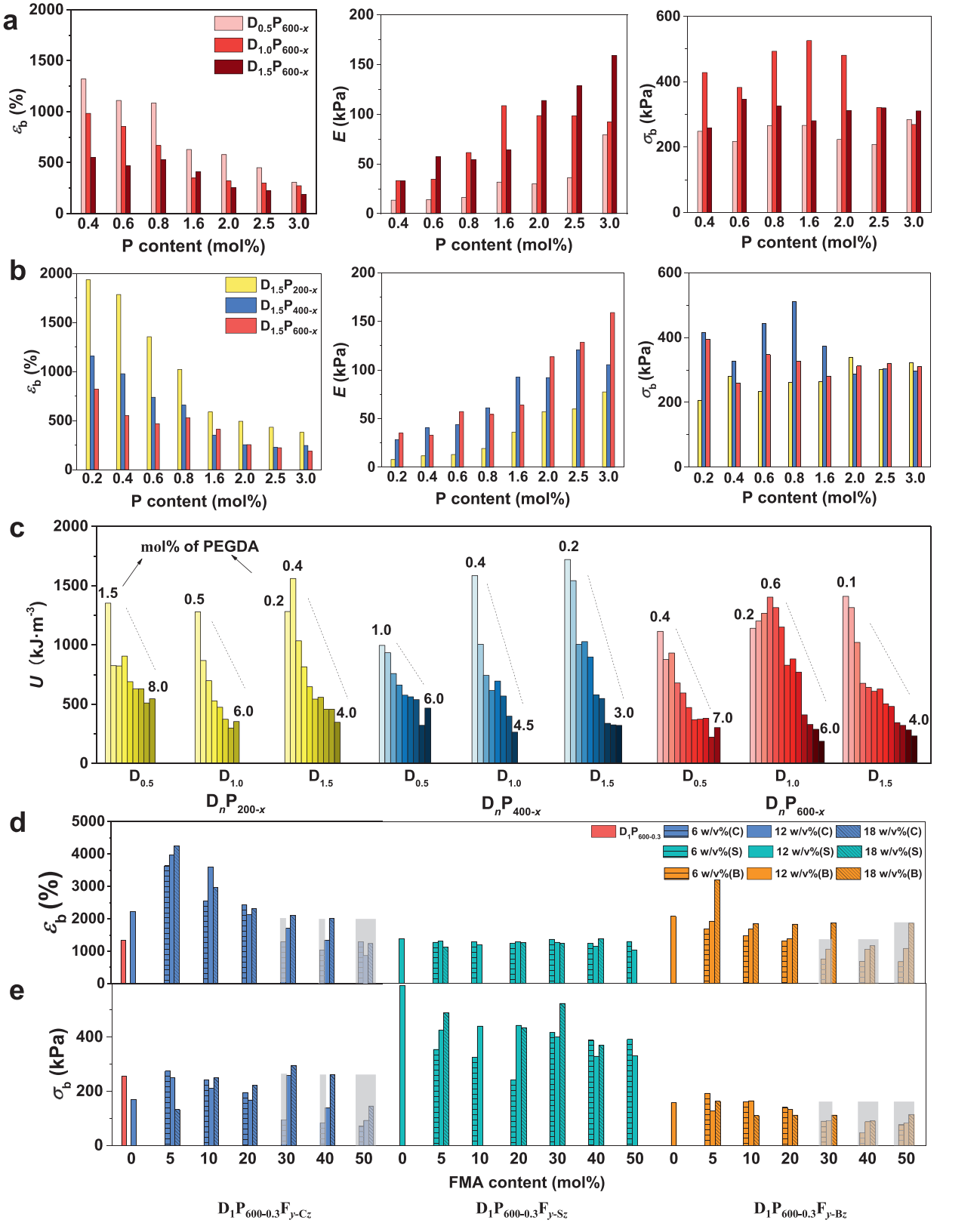

Figure 2. Mechanical properties of PPSB and PPSB-HA hydrogels. a,b) Effects of monomer concentration, crosslinker content and crosslinker chain length on elongation at break, Young's modulus, and strength at break. c) Overlook of fracture toughness of all PPSB hydrogels. d,e) Effects of FMA and surfactants (CTAC, SDS, and BS-12) on elongation at break and strength at break (The data covered in shade are from samples with incompletely dissolved FMA).

Table 2. Composition for optimization of surfactants and hydrophobic monomer.

System[a)]	Surfactants	Surfactant concentration (w/v%)	FMA content [mol%]
$D_1P_{600-0.3}$	CTAC	6	5
	SDS	12	10
	BS-12	18	20
			30
			40
			50

[a)]58 combinations and stoichiometries.

The representative healable hydrogels reported in the last 5 years were summarized in terms of materials, mechanical properties, healing mechanisms and performance, and applications (Table S1, Supporting Information). The elongation at break of $D_1P_{600-0.3}F_{5-C6}$ is the second highest among the reported healable hydrogels and the strength at break of our hydrogels is at a high level (Figure S9, Supporting Information). More importantly, our hydrogels possess ≈100% self-healing efficiency at gentle conditions within 2 h while most of the current reported hydrogels require external stimuli or elevated temperature or long time for healing (Figure 3d).

Furthermore, the $D_1P_{600-0.3}$, $D_1P_{600-0.3}F_{5-C6}$, and $D_1P_{600-0.3}F_{5-S6}$ hydrogels exhibit thermo-responsive shape memory behavior (Figure 3e and Video S1, Supporting Information). The permanent shape of the samples was ringlike. The temporary shape was fixed by freezing the samples at 25 °C for 2 h or at −10 °C for 1 h. The hydrogels returned to their original shape within 20 s by immersing in a ≈75 °C water bath. The principle of the thermal-responsive shape memory effect is the dynamic dissociation and recombination of the ionic bonding.[42]

To better elaborate the mechanical properties and self-healing capability of the hydrogels, schematic representation of the original, scalpel-cut, and healed hydrogels is illustrated

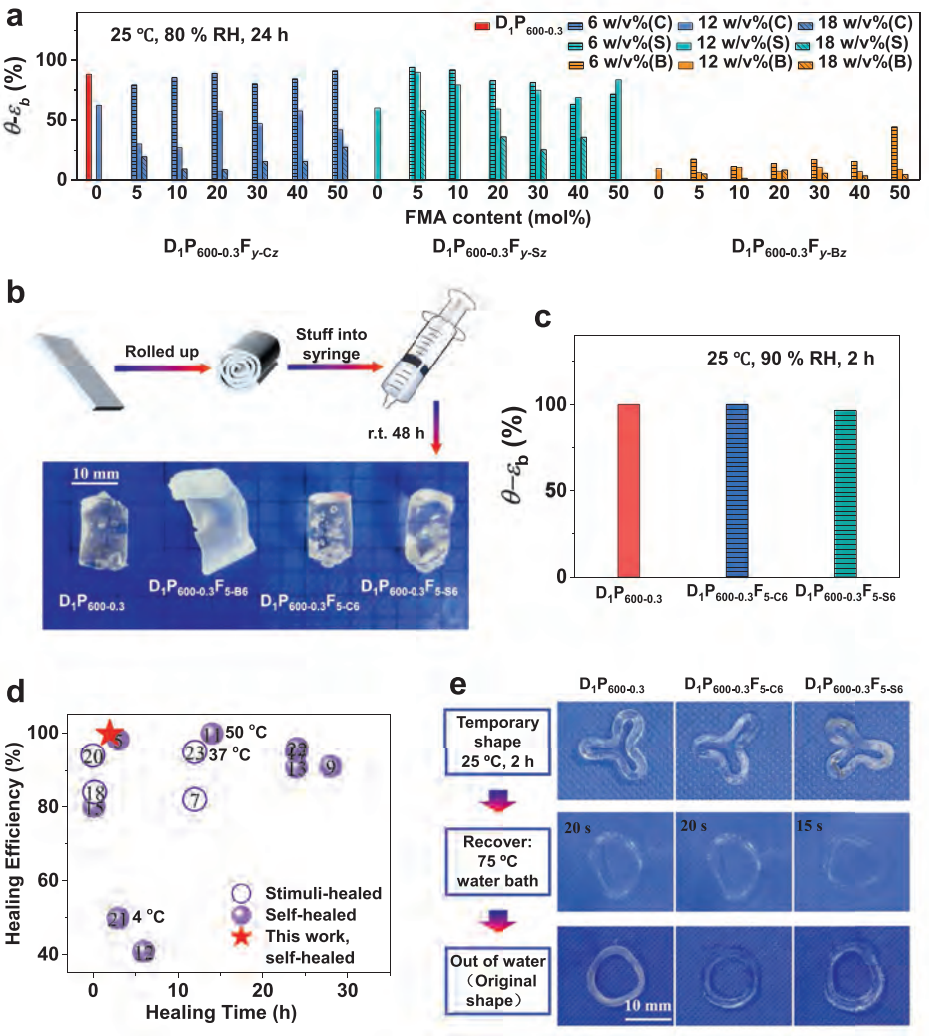

Figure 3. Self-healing properties of the PPSB-HA hydrogels. a) Self-healing efficiency in terms of elongation at break. b) Self-remolding properties of hydrogels (The pictures are from Video S1, Supporting Information). c) Self-healing properties of $D_1P_{600-0.3}$, $D_1P_{600-0.3}F_{5-C6}$, and $D_1P_{600-0.3}F_{5-S6}$ hydrogels under 90% RH. d) The comparison in self-healing properties of our hydrogel and representative self-healing hydrogels in the last 5 years. e) Shape memory effects of the $D_1P_{600-0.3}$, $D_1P_{600-0.3}F_{5-C6}$, and $D_1P_{600-0.3}F_{5-S6}$ hydrogels.

in **Figure 4**. For the PPSB hydrogels, there are intra-molecular and intra-group ionic bonding, large numbers of physical cross-links by inter-chain ionic bonding, and a small number of chemical crosslinks by PEGDA. When cut into two pieces, the cut surfaces are full of active free charges due to the super-hydrophilic nature of the polysulfobetaine materials. The dynamic ionic bonding immediately forms and the hydrogel returns to the original state upon reconnection. It is the recovery of a high proportion of ionic bonds that contributes to the high self-healing efficiency.

For PPSB-HA hydrogels, there are two types of micelles additionally: hybrid HA I with poly(FMA) inside surfactant micelles, and HA II containing pure surfactant molecules. HA I micelles bring multiple poly(DMAPS) chains together by the tightly entangled poly(FMA). HA micelles play a sacrificial role and enhance the toughness of the hydrogels; on the other hand, HA is auxiliary bonding in terms of self-healing. CTAC electrostatically attracts sulfonate anions (SO_3^-) at the end of the poly(DMAPS) side chains (Figure 4b). Therefore, CTAC micelles shrink the poly(DMAPS) chains resulting in higher elongation at break, which is well supported by the fact that the $D_1P_{600-0.3}F_{0-C12}$ sample (without FMA) possesses a larger ε_b than that of $D_1P_{600-0.3}$. The CTAC micelles with a small amount of poly(FMA) can be elongated easily through stretching the poly(FMA) chains, thus endows hydrogel network with distinguished stretchability (high ε_b). Nevertheless, the increase of FMA inside the micelles leads to chain entanglement, resulting in decreased elongation at break and slightly increased modulus. The toughening mechanism of the PPSB-HA/SDS hydrogels lies in the enhancement of interchain ionic bonding (Figure 4c). In principle, sulfate ions (SO_4^-) from SDS have stronger affinity to quaternary ammonium ions (NR_4^+) than SO_3^- from DMAPS. NR_4^+ ions of DMAPS position close to the polymer backbone; the negative charges of the SDS micelles show strong repulsion to the SO_3^- groups of poly(DMAPS). The ultimate effect is the elongated poly(DMAPS) chains, the reduction of intra-chain ionic bonds, the formation of strong interchain ionic bonding, and the exposure of intragroup ion pairs. The exposure of intragroup ion pairs can be verified from the superb water-absorption properties shown in Figure S10, Supporting Information. Consequently, when subjected to external force, the PPSB-HA/SDS hydrogels exhibit a larger E and

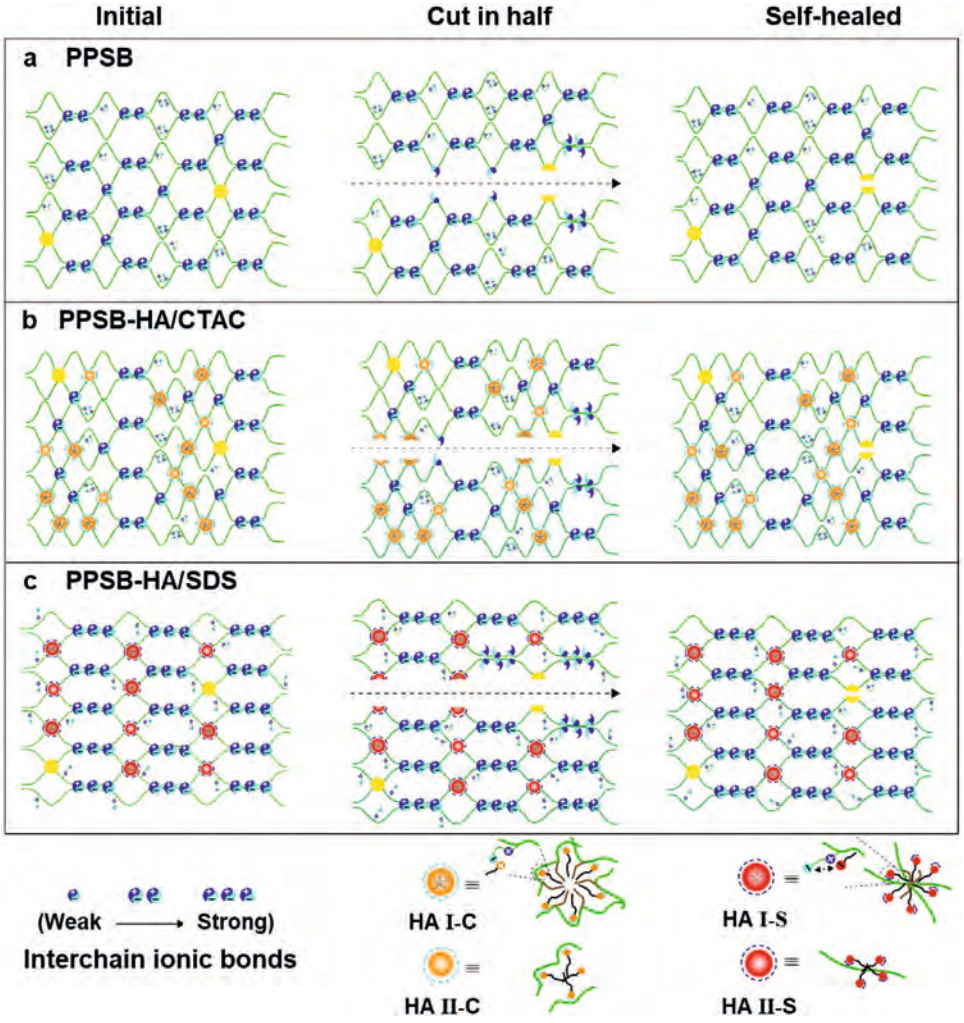

Figure 4. Illustration of the original, scalpel-cut, and self-healed states of the a) PPSB hydrogels, b) PPSB-HA hydrogels with CTAC, and c) PPSB-HA hydrogels with SDS.

higher σ_b compared with $D_1P_{600-0.3}$ (Figure 2c,d). The illustration of the PPSB-HA/BS-12 hydrogels is shown and analyzed in Figure S11, Supporting Information.

When the PPSB-HA hydrogels are cut in two halves, the newly generated interfaces consist of damaged micelles, dissociated hydrophobic segments, and separated ions. When reconnected together, the reunion of ion pairs and hydrophobic segments efficiently repairs the damaged interface. However, the ionic surfactant molecules form ionic bonding with the polymer segments, thus diluting the inter-chain ionic bonds and diminishing self-healing performance (Figure 3a). Compared with HA II micelles, HA I micelles with poly(FMA) possess stronger HA contributed to the improved self-healing properties. As a result, when the surfactant concentration is low (6 w/v%), the negative impacts on self-healing are limited (self-healing efficiency is higher than 80%); and when the concentration of surfactant is high (18 w/v%), self-healing properties are dramatically impaired but could be slightly made up by increasing the FMA content.

The above evaluation regarding the influence of monomers, crosslinkers, FMA and surfactants on hydrogel properties is solid and convincing because the conclusion is based on a large amount of experimental data facilitated by high throughput methodology. A designing guideline of self-healable zwetterionic hydrogels is suggested and presented in Figure S12, Supporting Information. Self-healing performance would be diminished by chain entanglement as well as chemical crosslinking. Elongation at break could be dramatically enlarged by introducing scarified bonding, such as hydrophobic association. Modulus would be enhanced by strong interactions and reduced by weak bonding. Strength at break representing the ability to withstand tension is usually determined by the strong interaction of the materials.

The self-healing capability does not lose when the hydrogels are properly functionalized. The $D_1P_{600-0.3}F_{5-C6}$ and $D_1P_{600-0.3}$ hydrogels were doped with PEDOT:PSS for high electrical conductance and their self-healing performances were evaluated. As shown in **Figure 5**a and Video S2, Supporting Information, a piece of $D_1P_{600-0.3}F_{5-C6}$-PEDOT:PSS hydrogel strip (both as-prepared and self-healed) serving as conductor connected to a circuit remains conducting as it was stretched up to 1500%, and as a result, a light emitting diode (LED) bulb in this circuit remained on during the stretch of the hydrogel. The $D_1P_{600-0.3}$-PEDOT:PSS hydrogel presents fast recovery in electrical conduction as well as mechanical properties, as demonstrated in Figure 5b. Before cutting, electrical conductivity of the sample was around 0.45 S cm^{-1}, and gradually decreased to 0.27 S cm^{-1} when the sample was stretched to 300%. After the hydrogel was cut into two pieces and in situ self-healed for ≈5 min, the conductance recovered to the original value, and the electrical conduction can largely maintain when another 4 cycles of stretching were applied. This sample ruptured until it was stretched to 700%.

Self-healable electronics requires all layers in the device to rapidly recover both mechanically and electrically. Here, hydrogels with different functions were applied to construct a self-healable capacitive-type e-skin, which consists of two silver nanowires (AgNWs)/$D_1P_{600-0.3}F_{5-C6}$ electrodes sandwiching a $D_1P_{600-1.2}$-PEDOT:PSS hydrogel with a microstructured surface. The AgNWs/$D_1P_{600-0.3}F_{5-C6}$ electrodes as well as the $D_1P_{600-1.2}$-PEDOT:PSS hydrogel dielectric were investigated to evaluate their self-healing performance. The AgNWs/$D_1P_{600-0.3}F_{5-C6}$ electrode displays real-time self-healing capability as demonstrated in Figure 5c and Video S3, Supporting Information. The electrode was first cut into two segments, which leads to the extinguishment of the LED bulbs connected to the circuit. Upon reconnection, the LED bulbs shine immediately and the hydrogel could be stretched to 100% strain after 30 s of self-healing, and restored to the initial conductance within 28 s after release. The $D_1P_{600-1.2}$-PEDOT:PSS hydrogel was selected as the dielectric layer of the device because hydrogel with crosslinker content of 1.2 mol% possess relatively higher Young's modulus for fast response speed (compare with $D_1P_{600-0.3}$), as presented in the database (Figure S2, Supporting Information). Surface microstructures has proven effectiveness in improving the sensitivity and response speed of pressure sensors, and thereby the top surface of the dielectric was made rough by introducing a graded intrafillable architecture molded from a piece of sandpaper (Figure S13, Supporting Information).[43] This microstructured hydrogel with higher rigidity also exhibited good self-healing performance even if the segments were reconnected with intentional mismatch (Figure 5d,e). Since all materials in the sensor were proven self-healable, we constructed an e-skin using the AgNWs/$D_1P_{600-0.3}F_{5-C6}$ electrodes and the $D_1P_{600-1.2}$-PEDOT:PSS dielectric. The device structure is shown in Figure 5f. An exceptional advantage of the e-skin is its fast and spontaneous self-healing capability at ambient condition: after the whole device was cut into two pieces, the e-skin functioned again within ≈9 min of healing (Figure 5g). To our best knowledge, intrinsically healable capacitive-type pressure sensors with high recovering efficiency and fast healing speed have not yet been reported elsewhere. By contrast, another reported self-healable multilayered electronics required 12 h for healing from the complete cutting off of the whole device.[44] Such an e-skin is expected to provide artificial limb and soft robotics with tactile sensing.

3. Conclusion

High-throughput screening technique has been used in the systematic investigation on the composition-property relationship of polysulfobetaine hydrogels. The effects of eight components were examined and over 150 combinations are proven to form hydrogels, and their properties are studied and compared. By employing the high-throughput screening method, hydrogels with elongation at break of ≈4000%, strength at break of ≈400 kPa, and self-healing efficiency ≈100% are attained. By incorporating the hydrogels with PEDOT:PSS and AgNWs, intrinsically stretchable and self-healable conductors are achieved and successful applied in LED circuit and pressure sensor. The polysulfobetaine hydrogel-based conductors as well as electronic skin exhibit impressively fast self-healing performance under ambient conditions. The unique combined properties of hydrogels will dramatically promote the advances of hydrogel-based electronics and their applications in wearable and implantable electronics. A high throughput characterization method is desired to boost the discovery and optimization

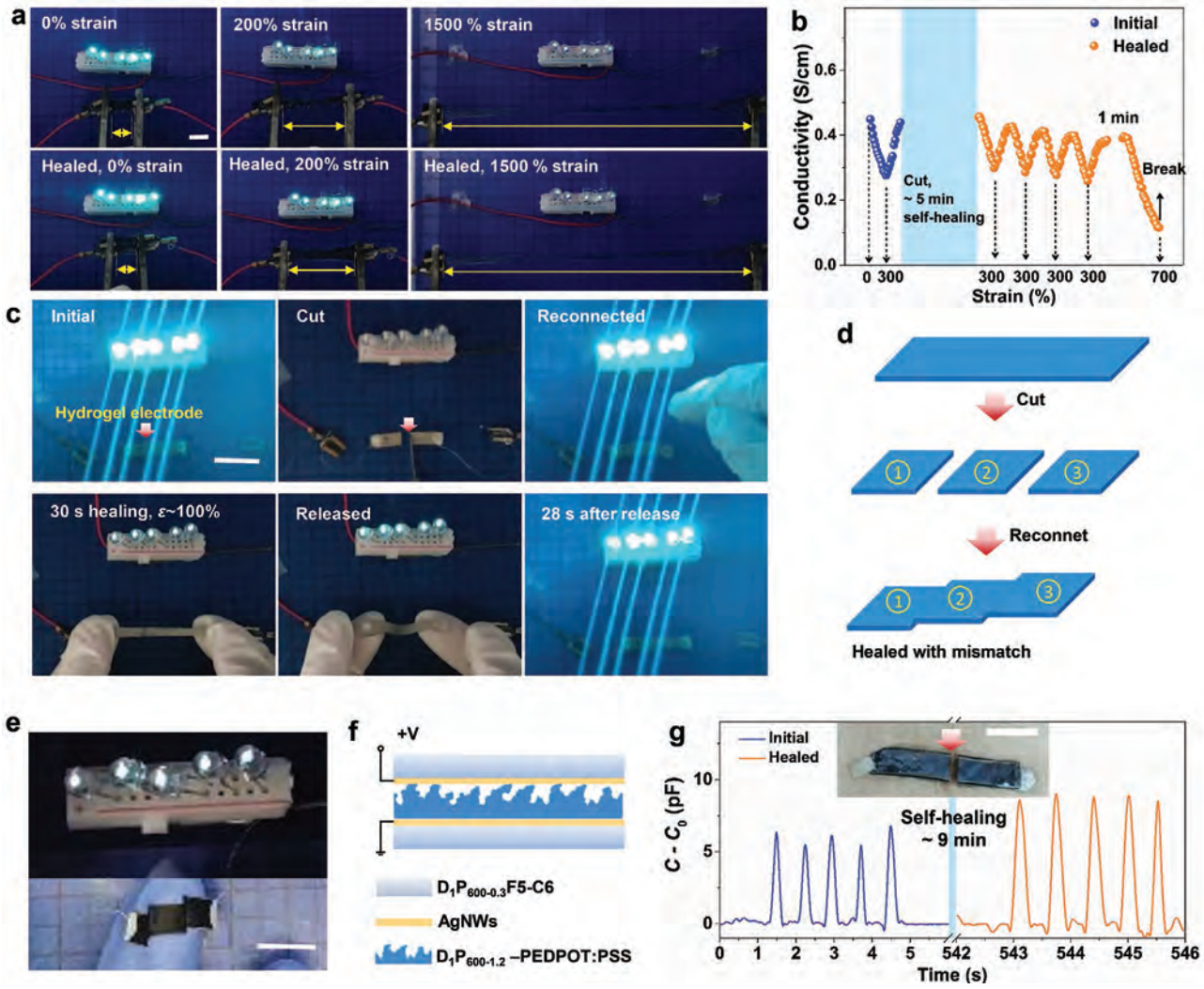

Figure 5. Self-healing of the hydrogel electrode and hydrogel-based electronic devices. a) $D_1P_{600\text{-}0.3}F_{5\text{–}C6}$-PEDOT:PSS hydrogels (top: as prepared, bottom: cut and self-healed at 25 °C and 90% RH) connected to an LED in series and stretched up to 1500% strain. b) Self-healing properties of the $D_1P_{600\text{-}0.3}$-PEDOT:PSS hydrogel at a minute level. c) Self-healing performance of the AgNWs/$D_1P_{600\text{–}0.3}$ electrode. d,e) Schematic illustration and photographs for the self-healing of intentional mismatch of the $D_1P_{600\text{–}1.2}$-PEDOT:PSS hydrogel with surface microstructures templated from sandpaper. f) Schematic device structure of the hydrogel-based capacitive sensor. g) Response to applied pressure of the sensor before cutting and after self-healing for 9 min (insert: photo image showing that the sensor is cut. Arrows indicate the cut interface). All scales in the figure is 1 cm.

of novel self-healable hydrogels with desired mechanical properties and multi-functionalities, which is the future development direction of high-throughput technologies.

4. Experimental Section

Materials: DMAPS (≥98.5%), PEGDA, APS, and FMA (98%) were purchased from Aladdin. lauryl betaine (BS-12, 30w/v% in water), CTAC (97%), and sodium dodecyl sulfate (SDS, ≥98.5%) were obtained from Bide. PEDOT:PSS (PH 1000, ≈1–1.3 wt% in water) was obtained from Xi'an Polymer Light Technology Corp. PDMS base (Sylgard 184) and corresponding curing agent were purchased from Dow Corning Co., Ltd. AgNWs was from XFNANO INC. All chemicals were used as received.

High Throughput Synthesis: For PPSB hydrogels, stock solutions of DMAPS (2.5 M), PEGDA (0.15 M for P200, 0.1125 M for P400, 0.056 M for P600) and APS (0.025 M) as well as deionized water were injected into square molds via computer-control syringes. The solution mixtures were mixed with ultrasonic vibration. Each sample differs from each other in DMAPS concentration, PEGDA types and content. APS content was 1 mol% to DMAPS for all hydrogels. The solutions were heated at 60 °C water bath under inert atmosphere for 18 h. Then the samples were kept in 25 °C and 80% RH (constant temperature and humidity incubator, HWS-80B, Shanghai, China) for 48 h before subjected to characterization. For PPSB-HA hydrogels, the stock solutions were DPA (mixture of DMAPS, P600, and APS), FMA, surfactant SDS/CTAC/BS-12 (30 w/v%) and deionized water. The synthesis was conducted under the same steps and condition as that of PPSB.

The hydrogels were noted as $D_nP_{a\text{–}x}F_{y\text{–}bz}$, where n is molar concentration of DMAPS (n = 0.5, 1, 1.5 mol L^{-1}); a refers to molecular weight of PEGDA (a = 200, 400, 600); x stands for the molar percentage of PEGDA related to DMAPS (x = ≈0.05–8 mol%); y (y = ≈5–50 mol%) stands for the molar percentage of FMA related to DMAPS, b (b = C/S/B, with C refers to CTAC, S to SDS, and B to BS-12) and z (z = 6/12/18 w/v%) refers to surfactant type and corresponding volume mass fraction in the hydrogels, respectively.

Synthesis of Conductive PPSB and PPSB-HA Hydrogels: The reaction conditions and reagents were the same as synthesis of PPSB and PPSB-HA hydrogels except that deionized water was replaced by PEDOT:PSS solution. The final PEDOT:PSS content was around 1.6 and 1.3 wt% in PPSB and PPSB-HA hydrogels, respectively.

Tensile Test: The hydrogels were cut into dumbbell-shape with the size of length 35 mm (L), gauge length 12 mm (l_0), and width 2 mm (w). Uniaxial stretching was performed with XLD-20E, Jingkong Mechanical testing Co., Ltd at a stretch velocity of 30 mm min^{-1}. Fracture toughness[45] was the integral area of stress–strain curves. Young's modulus was calculated by the slope of the linear fit from the stress–strain curves between ≈5–15% strain. All the mechanical tests were conducted under room temperature in air.

Self-Healing Property: The hydrogels were cut into two pieces and reconnected together subsequently for 24 h at 25 °C and 80% RH, then characterized with tensile test at dumbbell shape. The self-healing efficiency θ–ε_b was quantitatively defined as the elongation at break percentage of self-healed and original hydrogels. Self-healing property of PEDOT:PSS containing conductive gels was verified by lighting up LED in a series circuit powered by three commercial 1.5 V dry batteries. The conductivity of $D_1P_{600-0.3}$ hydrogels was calculated from the resistance measured with a digit multimeter (KEITHLEY 2100 6 1/2); the width and thickness of the sample were 5 and 2 mm respectively; the distance between probes was 10 mm.

Fabrication and Characterization of e-Skin: The sensor consists of two pieces of AgNWs/$D_1P_{600-0.3}$ electrodes sandwiching a $D_1P_{600-1.2}$-PEDOT:PSS hydrogel with surface microstructure. AgNWs were sprayed on the $D_1P_{600-0.3}$ with a silver jet (AC-27). The microstructure was molded from commercial sandpaper (roughness of no. 600#). Sandpaper was fixed on a substrate with taps. PDMS base was mixed with the curing agent at a weight ratio of 10:1. The uncured PDMS was poured on the sandpaper and cured for 12 h at ambient condition. Then the peel-off PDMS was fixed on silica gel box acting as a second molding template. DMAPS, PEGDA, APS, and PEDOT:PSS mixed solution was casted on the PDMS template and reacted at 60 °C under inert atmosphere for 18 h. More details concerning the microstructure and tests of corresponding sensor can be found in the previous paper.[43] All capacitance measurements were conducted with an LCR meter (Keysight E4980AL) at 0.1 MHz.

Supporting Information

Supporting Information is available from the Wiley Online Library or from the author.

Acknowledgements

Y.D. and H.T. contributed equally to this work. This work was financially supported by the funds of the National Key Research and Development Program of China (2018YFB0704100), the Key-Area Research and Development Program of Guangdong Province (2019B010941001), Shenzhen Clean Energy Research Institute Project (CERI-KY-2019-003), the High-level Special Funds (Grant Nos. G02256401, G02256301), National Key Project of Research and Development Plan (Grant Nos. 2017YFB0701900, 2018YFB0703600), the "Guangdong Innovative and Entrepreneurial Research Team Program" under contract no. 2016ZT06G587, the National Natural Science Foundation of China (no. 51771089), the "Science Technology and Innovation Committee of Shenzhen Municipality" (grant no. JCYJ20170817111714314), National Natural Science Foundation of China (81971764), Guangdong Research Fund (2019ZT08Y191). X.-D.X was supported by the fund of Guangdong Provincial Key Laboratory (Grant No. 2018B030322001) and the Guangdong-Hong Kong-Macao Joint Laboratory (Grant No. 2019B121205001).

Conflict of Interest

The authors declare no conflict of interest.

Data Availability Statement

Research data are not shared.

Keywords

high-throughput synthesis, hydrogels, polysulfobetaine, self-healable e-skin, self-healing hydrogels

Received: January 17, 2021
Published online:

[1] H. Yuk, B. Lu, X. Zhao, *Chem. Soc. Rev.* **2019**, *48*, 1642.
[2] H. Yuk, C. E. Varela, C. S. Nabzdyk, X. Mao, R. F. Padera, E. T. Roche, X. Zhao, *Nature* **2019**, *575*, 169.
[3] J. Deng, H. Yuk, J. Wu, C. E. Varela, X. Chen, E. T. Roche, C. F. Guo, X. Zhao, *Nat. Mater.* **2020**, *20*, 229.
[4] Y. Guo, J. Bae, Z. Fang, P. Li, F. Zhao, G. Yu, *Chem. Rev.* **2020**, *120*, 7642.
[5] S. Lin, X. Liu, J. Liu, H. Yuk, H.-C. Loh, G. A. Parada, C. Settens, J. Song, A. Masic, G. H. McKinley, X. Zhao, *Sci. Adv.* **2019**, *5*, eaau8528.
[6] C. Yang, Z. Suo, *Nat. Rev. Mater.* **2018**, *3*, 125.
[7] R. Macarron, M. N. Banks, D. Bojanic, D. J. Burns, D. A. Cirovic, T. Garyantes, D. V. S. Green, R. P. Hertzberg, W. P. Janzen, J. W. Paslay, U. Schopfer, G. S. Sittampalam, *Nat. Rev. Drug Discovery* **2011**, *10*, 188.
[8] R. A. Houghten, *Proc. Natl. Acad. Sci., U. S. A.* **1985**, *82*, 5131.
[9] W. F. Maier, *ACS Comb. Sci.* **2019**, *21*, 437.
[10] X. D. Xiang, G. Briceno, K. A. Wang, P. G. Schultz, X. Sun, Y. Lou, H. Chang, W. G. Wallace-Freedman, S. W. Chen, *Science* **1995**, *268*, 1738.
[11] G. Briceno, H. Y. Chang, X. D. Sun, P. G. Schultz, X. D. Xiang, *Science* **1995**, *270*, 273.
[12] J. Wang, Y. Yoo, C. Gao, I. I. Takeuchi, X. Sun, H. Chang, X. Xiang, P. G. Schultz, *Science* **1998**, *279*, 1712.
[13] X. Sun, K. Wang, Y. Yoo, W. Wallacefreedman, C. Gao, X. Xiang, P. G. Schultz, *Adv. Mater.* **1997**, *9*, 1046.
[14] S. A. Schunk, N. Böhmer, C. Futter, A. Kuschel, E. Prasetyo, T. Roussière, in *Catalysis*, (Eds: J. J. Spivey, K. M. Dooley, Y.-F. Han), Vol. *25*, The Royal Society of Chemistry, London **2013**, pp. 172–215.
[15] S. Chen, L. Zhang, L. Yan, X. Xiang, X. Zhao, S. Yang, B. Xu, *Adv. Funct. Mater.* **2019**, *29*, 1905487.
[16] S. Langner, F. Häse, J. D. Perea, T. Stubhan, J. Hauch, L. M. Roch, T. Heumueller, A. Aspuru-Guzik, C. J. Brabec, *Adv. Mater.* **2020**, *32*, 1907801.
[17] R. Potyrailo, K. Rajan, K. Stoewe, I. Takeuchi, B. Chisholm, H. Lam, *ACS Comb. Sci.* **2011**, *13*, 579.
[18] B. Lin, J. L. Hedrick, N. H. Park, R. M. Waymouth, *J. Am. Chem. Soc.* **2019**, *141*, 8921.
[19] T. R. Boussie, C. Coutard, H. Turner, V. Murphy, T. S. Powers, *Angew. Chem., Int. Ed.* **1998**, *37*, 3272.
[20] T. Janoschka, M. D. Hager, U. S. Schubert, *Adv. Mater.* **2012**, *24*, 6397.
[21] J. C. Meredith, A. Karim, E. J. Amis, *MRS Bull.* **2002**, *27*, 330.
[22] S. Wang, M. W. Urban, *Nat. Rev. Mater.* **2020**, *5*, 562.

[23] J. Qu, X. Zhao, Y. Liang, T. Zhang, P. X. Ma, B. Guo, *Biomaterials* **2018**, *183*, 185.
[24] B. L. Zhang, P. Zhang, H. Z. Zhang, C. Yan, Z. J. Zheng, B. Wu, Y. Yu, *Macromol. Rapid Commun.* **2017**, *38*, 1700110.
[25] A. J. D'Angelo, M. J. Panzer, *Chem. Mater.* **2019**, *31*, 2913.
[26] H. Jiang, L. Duan, X. Ren, G. Gao, *Eur. Polym. J.* **2019**, *112*, 660.
[27] M. W. Urban, D. Davydovich, Y. Yang, T. Demir, Y. Zhang, L. Casabianca, *Science* **2018**, *362*, 220.
[28] C.-H. Li, C. Wang, C. Keplinger, J.-L. Zuo, L. Jin, Y. Sun, P. Zheng, Y. Cao, F. Lissel, C. Linder, X.-Z. You, Z. Bao, *Nat. Chem.* **2016**, *8*, 618.
[29] D. L. Taylor, M. In, H. Panhuis, *Adv. Mater.* **2016**, *28*, 9060.
[30] B. Li, Z. Yuan, P. Jain, H.-C. Hung, Y. He, X. Lin, P. McMullen, S. Jiang, *Sci. Adv.* **2020**, *6*, eaba0754.
[31] K. He, Z. Liu, C. Wan, Y. Jiang, T. Wang, M. Wang, F. Zhang, Y. Liu, L. Pan, M. Xiao, H. Yang, X. Chen, *Adv. Mater.* **2020**, *32*, 2001130.
[32] T. Bai, S. J. Liu, F. Sun, A. Sinclair, L. Zhang, Q. Shao, S. Y. Jiang, *Biomaterials* **2014**, *35*, 3926.
[33] J. Ning, K. Kubota, G. Li, K. Haraguchi, *React. Funct. Polym.* **2013**, *73*, 969.
[34] X. Zhao, *Soft Matter* **2014**, *10*, 672.
[35] F. Wang, R. A. Weiss, *Macromolecules* **2018**, *51*, 7386.
[36] J. Xu, X. Ren, G. Gao, *Polymer* **2018**, *150*, 194.
[37] U. Gulyuz, O. Okay, *Macromolecules* **2014**, *47*, 6889.
[38] C. Bilici, V. Can, U. Nochel, M. Behl, A. Lendlein, O. Okay, *Macromolecules* **2016**, *49*, 7442.
[39] M. P. Algi, O. Okay, *Eur. Polym. J.* **2014**, *59*, 113.
[40] L. Wang, G. Gao, Y. Zhou, T. Xu, J. Chen, R. Wang, R. Zhang, J. Fu, *ACS Appl. Mater. Interfaces* **2019**, *11*, 3506.
[41] R. Lalani, L. Liu, *Polymer* **2011**, *52*, 5344.
[42] G. Jiang, C. Liu, X. Liu, Q. Chen, G. Zhang, M. Yang, F. Liu, *Polymer* **2010**, *51*, 1507.
[43] N. Bai, L. Wang, Q. Wang, J. Deng, Y. Wang, P. Lu, J. Huang, G. Li, Y. Zhang, J. Yang, K. Xie, X. Zhao, C. F. Guo, *Nat. Commun.* **2020**, *11*, 209.
[44] J. H. Kang, D. Son, G. J. N. Wang, Y. X. Liu, J. Lopez, Y. Kim, J. Y. Oh, T. Katsumata, J. W. Mun, Y. Lee, L. H. Jin, J. B. H. Tok, Z. N. Bao, *Adv. Mater.* **2018**, *30*, 1706846.
[45] G. R. Gao, G. L. Du, Y. N. Sun, J. Fu, *ACS Appl. Mater. Interfaces* **2015**, *7*, 5029.